nature photonics

LETTERS

PUBLISHED ONLINE: 18 APRIL 2010 | DOI: 10.1038/NPHOTON.2010.86

Room-temperature polariton lasing in an organic single-crystal microcavity

S. Kéna-Cohen[1,2] and S. R. Forrest[2]*

The optical properties of organic semiconductors are almost exclusively described using the Frenkel exciton picture[1]. In this description, the strong Coulombic interaction between an excited electron and the charged vacancy it leaves behind (a hole) is automatically taken into account. If, in an optical microcavity, the exciton–photon interaction is strong compared to the excitonic and photonic decay rates, a second quasiparticle, the microcavity polariton, must be introduced to properly account for this coupling[2]. Coherent, laser-like emission from polaritons has been predicted to occur when the ground-state occupancy of polaritons $\langle n_{gs} \rangle$, reaches 1 (ref. 3). This process, known as polariton lasing, can occur at thresholds much lower than required for conventional lasing. Polaritons in organic semiconductors are highly stable at room temperature, but to our knowledge, there has as yet been no report of nonlinear emission from these structures. Here, we demonstrate polariton lasing at room temperature in an organic microcavity composed of a melt-grown anthracene single crystal sandwiched between two dielectric mirrors.

Polariton lasing and Bose–Einstein condensation (BEC) of polaritons have both recently been observed in inorganic semiconductors[4–6]. However, with the exception of the nitrides, the strong-coupling regime has only been reported at cryogenic temperatures in inorganic materials due to the small binding energy (~10 meV) typical of the extended Wannier–Mott excitons characteristic of these materials. In contrast, strongly coupled organic microcavities can readily be made to span the entire visible spectrum at room temperature due to the high binding energy (~1 eV) of Frenkel excitons. In this work, we demonstrate polariton lasing in the organic semiconducting crystal anthracene at room temperature and at a threshold below that of our best-case estimate for conventional photon lasing.

We find, on reaching threshold, that the emission shifts from a sublinear bimolecular quenched regime to a superlinear regime accompanied by a drastic reduction in the emission lifetime, spectral narrowing and a thermalization of the polariton distribution function. Angle-resolved photoluminescence indicates that the microcavity remains in the strong-coupling regime above threshold, suggesting the transition from incoherent polariton emission to polariton lasing[7]. Furthermore, our calculations suggest that if organic polaritonic structures approaching the thermodynamic limit[8] can be realized, coherent emission using direct electrical injection is possible—a regime that heretofore has been inaccessible to organic materials[9].

The microcavity used in this study, shown schematically in Fig. 1a, consists of a nominally 120-nm-thick crystalline anthracene film sandwiched between two, 12-period, SiN_x/SiO_2 distributed Bragg reflectors (DBRs)[10]. In anthracene, two excitonic resonances are present, polarized along the **a** and **b** crystal axes. This splitting of the molecular resonance results from the Coulomb interaction between the two inequivalent molecules in the unit cell (Fig. 1b)[11]. Both cavity photon polarizations can couple simultaneously to these resonances and their vibronic replicas, resulting in an anisotropic dispersion with multiple polariton branches[10,12–15]. The dispersion corresponding to the **b**-polarized resonance is shown in Fig. 1c.

To identify a threshold in the polariton ground-state occupation, the emission spectrum at 0° was measured as a function of the pump fluence, varied using a series of metallic neutral density filters (Fig. 2). Here, the sample was pumped non-resonantly with 150-fs, $\lambda = 360$ nm pulses at an angle of 10° from normal incidence. The inset shows the integrated area of the **b**-polarized lower polariton (LP_b) emission peak as a function of pump fluence. This emission transitions from sublinear at low fluence where it is dominated by bimolecular quenching, to superlinear above threshold ($P_{th} = 120$ nJ). Immediately below and above threshold, the intensity dependence is fit to a power law x^p, with $p = 0.49 \pm 0.02$ and $p = 2.10 \pm 0.07$, respectively. At the highest fluences, the emission intensity saturates. However, emission from the **a**-polarized lower polariton (LP_a) remains in the sublinear regime both below and above threshold (see Supplementary Information). We also observe a narrowing of the emission linewidth from 16.5 meV immediately below threshold to 11.5 meV above. Note that because the cavity thickness is intentionally varied over the sample area, the observed linewidth is broadened here due to spatial averaging (see Methods and Supplementary Information).

A small blueshift of the polariton is observed above threshold, but this does not seem to be related to exciton–exciton interactions as in the case of inorganic semiconductors. Depending on the detuning between the excitonic resonance and the cavity mode, the polariton will blue- or redshift towards 2.94 eV. By measuring spots with different detunings, we have observed nonlinear emission from both the **a**- and **b**-polarized lower polaritons (LP_a and LP_b), with the laser emission polarized accordingly. However, lasing is only observed when the detuning is such that the polariton ground state is located near 2.94 eV. This corresponds to the energetic separation between the exciton reservoir and the first vibronic sublevel of the molecular ground state. This suggests that the polariton ground state is directly populated from the reservoir.

To investigate the polariton population, angle-resolved photoluminescence was performed along the **a**-axis of the crystal with a detection cone of half angle $\theta = 4°$. Photoluminescence below threshold, at a pump fluence of $0.003P_{th}$, is shown in Fig. 3a. The observed peak positions are directly associated with the polariton dispersion, $E_{LP}(k_a, k_b = 0)$, where k_a and k_b are the wave vectors along the **a** and **b** crystal axes, respectively. Emission from LP_b is strongest and is transverse electric (TE) polarized, whereas emission from LP_a is transverse magnetic (TM) polarized. In both cases, emission is strongest at $\theta = 0°$ (corresponding to zero in-plane wave vector), and decreases monotonically with increasing angle.

[1]Department of Electrical Engineering, Princeton University, Princeton, New Jersey 08544, USA, [2]Departments of Electrical Engineering and Computer Science and Physics, University of Michigan, Ann Arbor, Michigan 48109, USA. *e-mail: stevefor@umich.edu

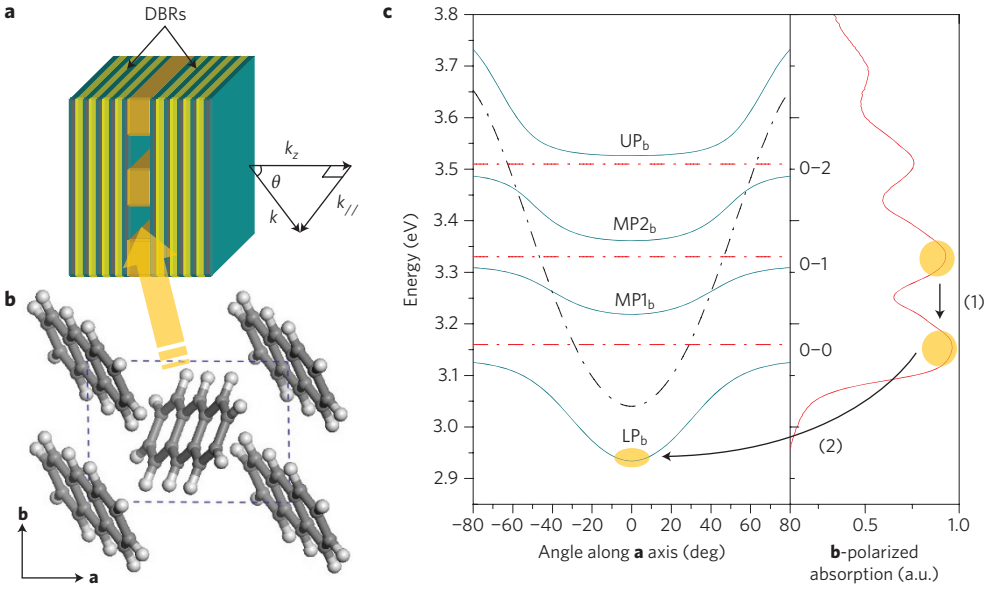

Figure 1 | Experimental structure and dispersion of the b-polarized polariton. a, Schematic showing the fabricated structure and empty channels before filling with anthracene. **b**, Anthracene crystal structure viewed along the [001] stacking direction. Two molecules per unit cell can be identified, and the **a** and **b** crystal axes are indicated. This results in two distinct polaritons having an anisotropic dispersion[10,12–15]. **c**, Left: calculated dispersion of the **b**-polarized polariton along the **a**-crystal axis. The lower polariton (LP_b), middle polaritons (MP_b) and upper polariton (UP_b) branches resulting from strong coupling of the cavity photon to the intramolecular vibronics are indicated. The bare (uncoupled) dispersions of the exciton and cavity photon are also shown (dashed-dotted lines). Each angle can be related to the in-plane wave vector k_a using the relation $k_a = (\omega/c)\sin\theta$, where ω is the radial light frequency, c is the speed of light and θ is the angle defined in **a**. Right: absorption spectrum of anthracene. Multiple resonances are seen, corresponding to the absorption of a photon accompanied by the creation of a molecular vibration. (1) Fast relaxation of the photogenerated excitons to the bottom of the excitonic band (reservoir) through the emission of optical phonons. (2) Direct pumping of the polaritonic ground state from the exciton reservoir.

This reflects the decreasing polariton population and increasing lifetime with increasing angle along the branch. The emission spot below threshold is shown in the inset of Fig. 3a. It is circular and Gaussian in intensity. The angle-resolved photoluminescence above threshold at a pump fluence of $1.3P_{th}$, shown in Fig. 3b, indicates that the dispersion is unchanged, confirming that the structure is still in the strong-coupling regime. However, the emission occurs almost exclusively from LP_b and becomes localized near the bottom of the branch. Furthermore, the emission spot changes drastically,

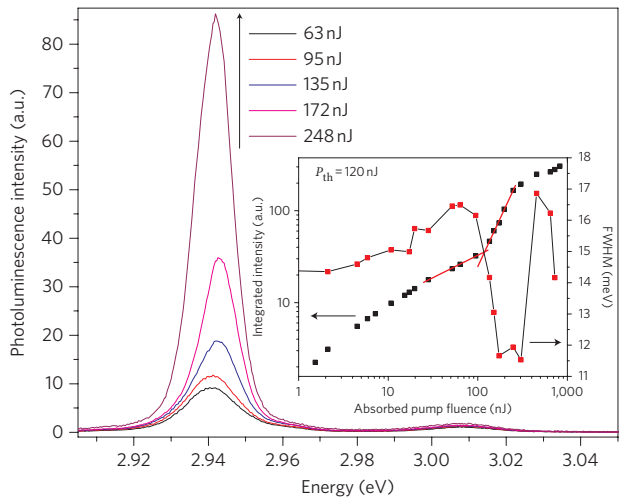

Figure 2 | Intensity dependence. Photoluminescence measured at $k = 0$ as a function of pump fluence. Inset: integrated area of LP_b and FWHM linewidth of LP_b at $k = 0$ as functions of pump fluence. The lasing threshold is defined as the intersection between the sublinear regime dominated by bimolecular quenching, and the superlinear region.

acquiring a Hermite–Gaussian TEM_{01} modal structure. In regions with a detuning where lasing does not occur, neither a modal structure nor bright spots are seen at the same pump intensity. The bright emission spots observed above threshold seem to be localized near structural inhomogeneities on the film, and the two modal lobes retain the same shape on various locations on the sample where lasing occurs. Similar transverse mode profiles have resulted from anisotropy in vertical-cavity surface-emitting lasers[16].

To determine the nature of the scattering mechanism responsible for populating the lower branch, we calculated the scattering rate of a reservoir exciton to the polariton ground state via the non-radiative emission of an optical phonon[17] to be $k_{nr} \approx (100\ \text{ns})^{-1}$ (using molecular density $\rho = 2/476.5\ \text{Å}^3$, exciton–phonon coupling constant $g \approx 1$ and detuning $\Delta = -120$ meV). This value is large compared to the radiative lifetime of anthracene, suggesting that radiative scattering, mediated by the dipole interaction, is dominant[18]. Note that, even below threshold, a peak in photoluminescence at an emission angle θ corresponding to $E_{LP}(\theta) \approx 2.94$ eV is observed[15], highlighting the effectiveness of this scattering mechanism. This behaviour is in striking contrast to inorganic semiconductors, in which relaxation occurs by means of multistep relaxation along the lower branch, and where exciton–exciton interactions play a crucial role in the scattering process[19].

The emission lifetime was measured with a streak camera using the same detection geometry. The time-dependence of the integrated intensity originating from LP_b is shown in Fig. 4a. At $0.018P_{th}$, the emission follows single-exponential decay at long times, with a lifetime $\tau = 1.04 \pm 0.02$ ns. At higher pump fluences, the emission lifetime is further reduced at short times, along with an increase in the influence of bimolecular quenching. Above threshold, the emission decay time collapses to <30 ps and is limited by the resolution of our experimental apparatus. The short emission lifetime above threshold is a result of effective scattering from the exciton reservoir to the bottom of the lower polariton

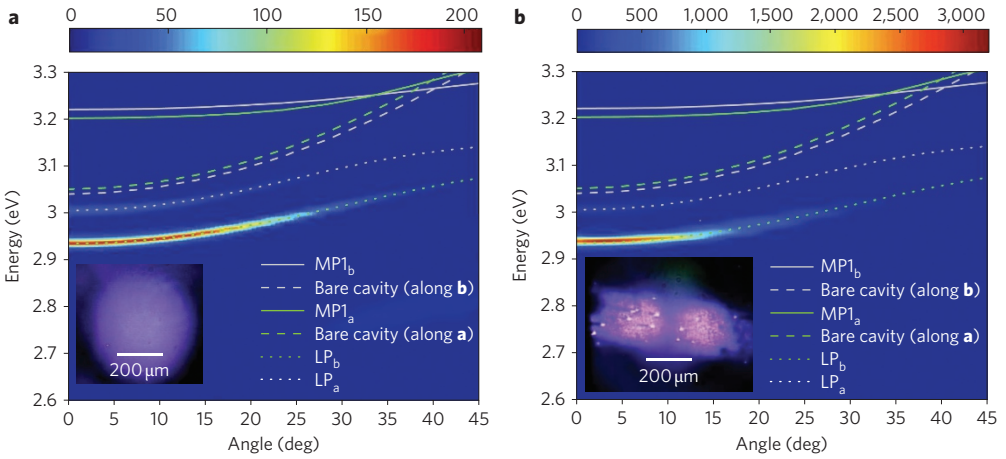

Figure 3 | Angle-resolved photoluminescence. a, Angle-resolved photoluminescence (PL) measured below threshold. Emission from LP_a and LP_b is observed. Dashed lines corresponding to the position of the 'uncoupled' cavity modes are indicated for reference. The solid line shows the position of $MP1_b$ (not observed in PL). **b**, Angle-resolved photoluminescence measured above threshold. Emission is seen to still occur from the lower polariton branches and not the 'uncoupled' cavity, providing strong evidence for polariton lasing. The insets show the emission spot imaged using a colour charge-coupled device camera below (**a**) and above (**b**) threshold. The **b**-axis is in the vertical direction.

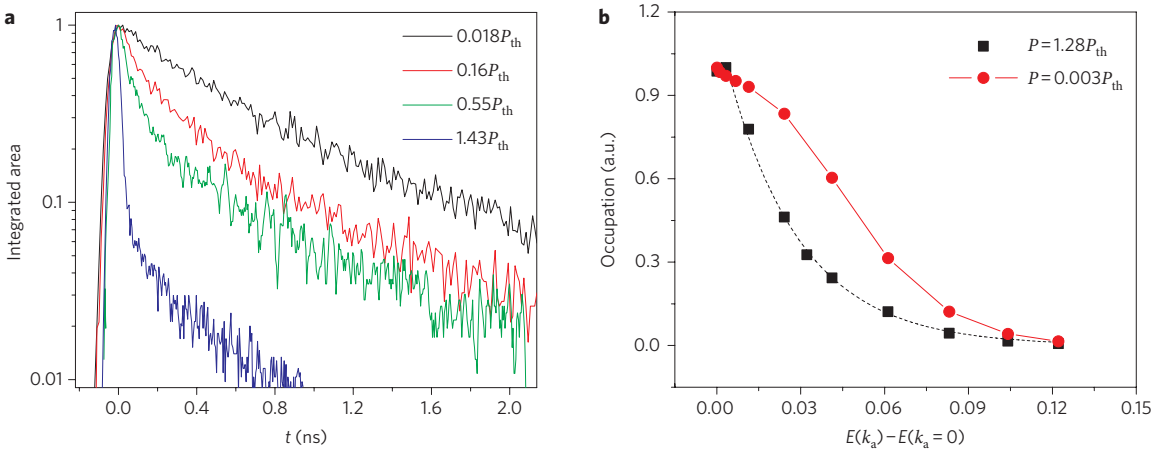

Figure 4 | Temporal response and occupation number. a, Normalized photoluminescence transient intensity taken in the normal direction ($\theta = 0^\circ$ in Fig. 1a) for increasing pump fluence, showing the evolution from weakly quenched, to strongly quenched, to lasing. The single-exponential decay time constant at low pump fluence (or long times) varies between 0.7 and 2.5 ns, depending on the probed spot due to variations in impurity and trap densities on the sample. The decay time, however, always collapses to <30 ps above threshold. **b**, Polariton distribution function below and above threshold. Above threshold, the distribution can be fit to a Boltzmann distribution: $n(E) \propto \exp(-\Delta E/k_B T_{lattice})$, where $\Delta E \equiv E(k_a) - E(k_a = 0)$ and k_B is Boltzman's constant. The fit results in a lattice temperature of $T_{lattice} = 326$ K.

branch, and the short cavity photon lifetime compared to the non-radiative polariton decay rate.

The lower polariton population density below and above threshold is shown in Fig. 4b. The shape of the polariton population density function is determined by the various scattering rates, and may or may not reach thermal equilibrium depending on the decay rate of polaritons compared to these rates. Below threshold, the system appears to be far from thermal equilibrium. Above threshold, the peak emission is found slightly off-normal at $\theta = 2.5^\circ$. Indeed, this angle provides the resonance condition for direct pumping from the reservoir. However, for higher angles, the population distribution changes to a shape that is indistinguishable from a Boltzmann distribution, with an activation energy corresponding to a lattice temperature $T_{lattice} = 326$ K. This suggests that relaxation above threshold is greatly enhanced and that even under pulsed excitation, some thermalization occurs. The population near $k = 0$, however, differs from that expected for a Bose–Einstein condensate at thermal equilibrium, and from Fig. 2, it is apparent that in anthracene, non-radiative decay by bimolecular annihilation severely limits the possibility of achieving extremely large ground-state populations.

The observation of stimulated emission from crystalline anthracene has been reported at low temperatures[20], but to our knowledge this is the first demonstration of lasing from crystalline anthracene. We can, nevertheless, estimate the pump density required for conventional photon lasing in the same structure. Figure 5 shows the amplified spontaneous emission (ASE) spectrum emitted from the facet of a neat anthracene crystal. By varying the dimensions of the pump spot, we have measured a gain coefficient $\alpha \approx 20$ cm^{-1} at a pump density of 43 μJ cm^{-2} (15.9 μJ cm^{-2} absorbed). In the microcavity, the mirror losses alone are calculated to be at least 540 cm^{-1} (see Supplementary Information). Assuming the best case where the gain scales linearly with the pump density (ignoring bimolecular quenching), we calculate a threshold $P_{th} = 430$ μJ cm^{-2} for conventional lasing. At threshold for polariton lasing, however, we measure an absorbed pump density of only $P_{th} = 320$ μJ cm^{-2}.

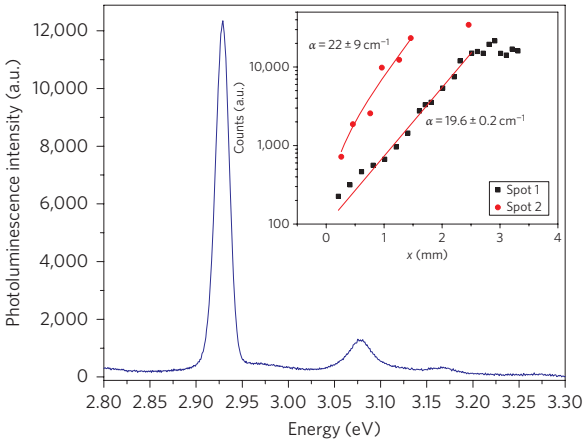

Figure 5 | Gain measurement. ASE spectrum collected from the facet of a 120-nm-thick anthracene single crystal. The inset shows the peak ASE intensity measured as a function of pump stripe length. To extract the gain $\alpha(\lambda)$, the data are fit to $I(\lambda) \propto \exp(\alpha(\lambda)L) - 1$ where $I(\lambda)$ is the ASE intensity and L is the stripe length. A value of $\sim$20 cm^{-1} is obtained.

However, the distinction between polariton and photon lasing remains subtle in this organic semiconductor. Unlike in the case of inorganic semiconductors, the Mott density is never exceeded in organic semiconductors (we know of no demonstration of a free electron–hole plasma in an organic material), and as a result, the polariton emission is never bleached. However, 'transparency' is always exceeded for vibronic sublevels of the ground state, because these are unoccupied in thermal equilibrium. Absorption occurs from the relaxed ground state to vibronic sublevels of the excited state, whereas spontaneous emission occurs from the relaxed excited state to vibronic sublevels of the ground state. Because the peak of the amplified spontaneous emission spectrum corresponds to these transitions, gain may be contributing to the radiative scattering mechanism that populates the polariton ground state.

In inorganic microcavities, the polariton lasing threshold has been found to be as much as one order of magnitude lower than that for conventional photon lasing. However, in organic crystals with inversion symmetry (for example, anthracene), only high-order multipoles contribute to the dynamic exciton–exciton interaction that is responsible for the efficient polariton–polariton scattering of inorganic semiconductors, making it relatively inefficient[21]. It is the large intramolecular phonon energy characteristic of organic materials, however, that enables direct pumping of the lower branch from the reservoir. Organic materials with efficient non-radiative scattering mechanisms such as exciton–phonon and exciton–exciton interactions may further reduce the polariton lasing threshold compared to that of conventional lasing. Indeed, we have calculated the phase diagram[8] of the experimental structure in the thermodynamic limit (assuming an infinite particle lifetime) and find a threshold density for condensation of $N_{th} = 3 \times 10^{13}$ cm^{-3} (see Supplementary Information). Direct electrical pumping of such a structure beyond threshold would be feasible with current organic light-emitting diode architectures[22].

In conclusion, we have observed room-temperature polariton lasing from a microcavity composed of an organic single crystal of anthracene sandwiched between two DBRs. The lasing threshold of $P_{th} = 320$ μJ cm^{-2} is lower than our best-case estimate of the threshold for conventional lasing. Efficient population of the ground state seems to be a result of direct radiative pumping from the reservoir. Spatial modulation of the pump spot, spectral narrowing, a collapse of the emission lifetime and a change in the polariton distribution function are observed on reaching threshold.

Methods

Experimental structure. Each DBR is composed of 12 alternating pairs of silicon dioxide (SiO_2, $n = 1.478$) and silicon nitride (SiN_x, $n = 1.947$). The centre of the DBR stopband is located at 410 nm. Before growing the films, 60-nm-thick gold stripes were evaporated onto each DBR. Opposing DBRs were bonded together, thus forming empty channels. Liquid anthracene was then allowed to penetrate the channels and was slowly cooled at a rate of 1 °C min^{-1} to form the single crystals. Further details regarding the fabrication have been reported in ref. 10. Angle-resolved reflectivity and photoluminescence for a 140-nm-thick cavity have been reported in refs 10 and 15. Here, the width of the channels was 2 mm, compared to 0.5 mm in previous reports, allowing us to probe spots of different detuning on the same sample due to a natural bowing of the channels.

Characterization. The pump pulses were generated from the fourth harmonic of the idler of an optical parametric amplifier (OPA). The OPA was pumped by a 1 kHz Ti:sapphire regenerative amplifier (Clark-MXR, CPA-2110), and the pulses were focused to a 220-μm-diameter full-width at half-maximum (FWHM) spot using a SiO_2 lens with a focal length of 50 cm. The $\lambda = 360$ nm pump wavelength was chosen to correspond approximately to the first transmission maximum beyond the edge of the DBR stopband. Because polariton emission was only observed from the **a**- and **b**-polarized lower branches (LP_a and LP_b), a $\lambda = 400$ nm long-wave pass dielectric filter was used to block any scattered pump light. Time-resolved measurements were performed using a Hamamatsu C4334 streak camera coupled to a monochromator. The camera was triggered using an optical signal derived from the seed oscillator, resulting in a timing jitter-limited resolution of 30 ps.

Polariton dispersion and occupation number. The polariton dispersion from Fig. 1c was modelled by a coupled harmonic oscillator Hamiltonian:

$$\begin{pmatrix} E_{ph}(\theta) & V_1 & V_2 & V_3 \\ V_1 & E_{ex0-0} & 0 & 0 \\ V_2 & 0 & E_{ex0-1} & 0 \\ V_3 & 0 & 0 & E_{ex0-2} \end{pmatrix} \begin{pmatrix} \alpha \\ \beta \\ \chi \\ \delta \end{pmatrix} = E \begin{pmatrix} \alpha \\ \beta \\ \chi \\ \delta \end{pmatrix} \quad (1)$$

Fit parameters were the same as in ref. 10 except for $V_1 = 128$ meV and $E_{ph}(0) = 3.04$ eV. Note that the dispersion is measured along **a**, in contrast to ref. 10 where it is measured along **b** (see ref. 15 for further explanation). From the coupled oscillator model, the photon fraction was extracted as a function of angle. This information was used to generate Fig. 4b using

$$N_{LP}(\theta) \propto \frac{I_{LP}}{\alpha(\theta)^2} \quad (2)$$

where I_{LP} is the integrated intensity, N_{LP} the population and α the photon fraction. To convert to occupation number, the data are then divided by $(\cos\theta)$ to correct for the fraction of detected states in momentum space.

Gain measurement. The gain of anthracene was measured using the variable stripe length method at two locations on an $L = 120$-nm-thick film enclosed between two quartz slides. The pump was focused onto the sample using a cylindrical lens, and a rectangular aperture was used to define a uniform rectangular region. The precise dimensions of the pump spot were measured using a laser beam profiler, and intensity modulations were at most ±20% over the entire area of the stripe. The sample and detector were translated into the beam, and the ASE spectrum was recorded as a function of position. We determined a value of $\sim$20 cm^{-1}. As a possible explanation for the Boltzmann occupancy above threshold, we also verified that the high-energy tail of the ASE spectrum is not thermalized.

Ground-state occupancy. The output power was measured at threshold with a high-sensitivity Joulemeter (3.224×10^8 V J^{-1}) behind the long-wave pass filter. From this, we could obtain an estimate of the ground-state occupancy in this system. We determined an output fluence of 0.2 ± 0.1 pJ. Ignoring the weak anisotropy, the total number of states within the detection cone was calculated as[5]

$$M = \frac{\pi D^2/4}{4\pi^2} \pi (k_0 \Delta\theta)^2 \quad (3)$$

where D is the spot diameter, $k_0 = 2\pi/\lambda$ and $\Delta\theta$ is the detection half-angle. We obtained an average occupancy $\langle n \rangle \approx 238$/state. This value is well above the $\langle n_{gs} \rangle \approx 1$ threshold required for polariton lasing. Note that the measured output power slightly overestimates the actual density because it includes contributions from LP_a and from the leaky modes of the DBR. The large discrepancy for this measurement originates from contributions other than LP_b, which needed to be subtracted. Notably, this includes the detector noise floor and weakly scattered light from the fundamental and the second harmonic of the idler.

Received 4 October 2009; accepted 12 March 2010; published online 18 April 2010

References

1. Pope, M., Swenberg, C. E. & Pope, M. *Electronic Processes in Organic Crystals and Polymers* 2nd edn (Oxford Univ. Press, 1999).
2. Lidzey, D. G. *et al.* Strong exciton–photon coupling in an organic semiconductor microcavity. *Nature* **395,** 53–55 (1998).
3. Imamoglu, A., Ram, R. J., Pau, S. & Yamamoto, Y. Nonequilibrium condensates and lasers without inversion: exciton–polariton lasers. *Phys. Rev. A* **53,** 4250–4253 (1996).
4. Kasprzak, J. *et al.* Bose–Einstein condensation of exciton polaritons. *Nature* **443,** 409–414 (2006).
5. Deng, H., Weihs, G., Snoke, D., Bloch, J. & Yamamoto, Y. Polariton lasing vs. photon lasing in a semiconductor microcavity. *Proc. Natl Acad. Sci. USA* **100,** 15318–15323 (2003).
6. Christopoulos, S. *et al.* Room-temperature polariton lasing in semiconductor microcavities. *Phys. Rev. Lett.* **98,** 126405 (2007).
7. Malpuech, G., Kavokin, A. & Laussy, F. P. Polariton Bose condensation in microcavities. *Phys. Status Solidi A* **195,** 568–578 (2003).
8. Malpuech, G., Rubo, Y. G., Laussy, F. P., Bigenwald, P. & Kavokin, A. V. Polariton laser: thermodynamics and quantum kinetic theory. *Semicond. Sci. Technol.* **18,** S395–S404 (2003).
9. Giebink, N. C. & Forrest, S. R. Temporal response of optically pumped organic semiconductor lasers and its implication for reaching threshold under electrical excitation. *Phys. Rev. B* **79,** 073302 (2009).
10. Kena-Cohen, S., Davanço, M. & Forrest, S. R. Strong exciton–photon coupling in an organic single crystal microcavity. *Phys. Rev. Lett.* **101,** 116401 (2008).
11. Davydov, A. S. *Theory of Molecular Excitons* (Plenum Press, 1971).
12. Zoubi, H. & La Rocca, G. C. Microscopic theory of anisotropic organic cavity exciton polaritons. *Phys. Rev. B* **71,** 235316 (2005).
13. Litinskaya, M., Reineker, P. & Agranovich, V. M. Exciton–polaritons in a crystalline anisotropic organic microcavity. *Phys. Status Solidi A* **201,** 646–654 (2004).
14. Kena-Cohen, S. & Forrest, S. R. Giant Davydov splitting of the lower polariton branch in a polycrystalline tetracene microcavity. *Phys. Rev. B* **77,** 073205 (2008).
15. Kena-Cohen, S., Davanco, M. & Forrest, S. R. Resonant Rayleigh scattering from an anisotropic organic single-crystal microcavity. *Phys. Rev. B* **78,** 153102 (2008).
16. Debernardi, P., Bava, G. P., Degen, C., Fischer, I. & Elsasser, W. Influence of anisotropies on transverse modes in oxide-confined VCSELs. *IEEE J. Quantum Electron.* **38,** 73–84 (2002).
17. Litinskaya, M., Reineker, P. & Agranovich, V. M. Fast polariton relaxation in strongly coupled organic microcavities. *J. Lumin.* **110,** 364–372 (2004).
18. Mazza, L., Fontanesi, L. & La Rocca, G. C. Organic-based microcavities with vibronic progressions: photoluminescence. *Phys. Rev. B* **80,** 235314 (2009).
19. Tassone, F. & Yamamoto, Y. Exciton–exciton scattering dynamics in a semiconductor microcavity and stimulated scattering into polaritons. *Phys. Rev. B* **59,** 10830–10842 (1999).
20. Avanesyan, O. S. *et al.* Features of light-emission and stimulated Raman-scattering in anthracene-crystals. *Soviet J. Quantum Electron.* **7,** 403–405 (1977).
21. Litinskaya, M. Exciton polariton kinematic interaction in crystalline organic microcavities. *Phys. Rev. B* **77,** 155325 (2008).
22. Tischler, J. R., Bradley, M. S., Bulovic, V., Song, J. H. & Nurmikko, A. Strong coupling in a microcavity LED. *Phys. Rev. Lett.* **95,** 036401 (2005).

Acknowledgements

The authors acknowledge fruitful discussions with H. Deng. This work was performed at the Lurie Nanofabrication Facility at the University of Michigan and was supported by Universal Display Corp. and the Air Force Office of Scientific Research.

Author contributions

S.K.C. and S.R.F conceived the experiments. S.K.C. fabricated the structures and carried out the measurements. Both authors contributed to the analysis and manuscript.

Additional information

The authors declare competing financial interests: details accompany the full-text HTML version of the paper at www.nature.com/naturephotonics. Supplementary information accompanies this paper at www.nature.com/naturephotonics. Reprints and permission information is available online at http://npg.nature.com/reprintsandpermissions/. Correspondence and requests for materials should be addressed to S.R.F.